

# Lawrence Berkeley National Laboratory

## Recent Work

### Title

Field Response of Magnetic Vortices in Dusty Olivine From the Semarkona Chondrite

### Permalink

<https://escholarship.org/uc/item/7116b9dj>

### Journal

Geochemistry, Geophysics, Geosystems, 20(3)

### ISSN

1525-2027

### Authors

Nichols, CIO

Einsle, JF

Im, MY

et al.

### Publication Date

2019-03-01

### DOI

10.1029/2018GC008159

Peer reviewed

# Field-response of magnetic vortices in dusty olivine from the Semarkona chondrite

Claire I. O. Nichols<sup>a,b\*</sup>, Joshua F. Einsle<sup>a,c</sup>, Mi-Young Im<sup>c</sup>, Peter Fischer<sup>c,d</sup>, Takeshi Kasama<sup>e</sup>, Zineb Saghi<sup>c,g</sup>, Richard J. Harrison<sup>a</sup>

\*cion2@mit.edu

<sup>a</sup>Department of Earth Sciences, University of Cambridge, Downing Street, Cambridge, CB2 3EQ, UK

<sup>b</sup>Department of Earth, Atmospheric and Planetary Sciences, MIT, Cambridge, MA, USA

<sup>c</sup>Department of Materials Science and Metallurgy, University of Cambridge

<sup>d</sup>Advanced Light Source, Lawrence Berkeley National Laboratory, Berkeley, CA, USA

<sup>e</sup>Physics Department, University of California Santa Cruz

<sup>f</sup>Centre for Electron Nanoscopy, Technical University of Denmark

<sup>g</sup>CEA, LETI, MINATEC Campus, F-38054 Grenoble, France

## Abstract

Recent paleomagnetic studies have constrained the strength and longevity of the magnetic field generated by the solar nebula, which has broad implications for the early evolution of the solar system. Paleomagnetic evidence was recorded by nanoscale iron inclusions in olivine crystals in the Semarkona LL 3.0 chondrite. These ‘dusty olivines’, have been shown to be credible carriers of ancient magnetic remanence. The small scale of the iron inclusions presents several challenges for defining their fundamental magnetic properties. Here we present the first correlative study of the response of these magnetic structures under applied laboratory fields. Results show that the majority of particles are in a single-vortex state and exhibit stable magnetic behaviour in applied fields  $\geq 200$  mT. Experimental observations using Lorentz microscopy and transmission X-ray microscopy are shown to compare well with the results of finite-element micromagnetic simulations derived from 3D models of the particles obtained using electron nanotomography. This correlative approach may be used to characterise the fundamental magnetic behaviour of many terrestrial and extraterrestrial paleomagnetic carriers in the single- to multi-vortex size range, which represent the vast majority of stable magnetic carriers in rocks and meteorites.

## Significance Statement

Characterising the fundamental rock magnetic properties of meteorites is of extreme importance when interpreting paleomagnetic signals from the early solar system. We present the first correlative study of dusty olivines from the Semarkona ordinary chondrite using X-ray and electron microscopy techniques combined with micromagnetic simulations to demonstrate their magnetic structure is stable in applied magnetic fields exceeding 200 mT. This supports previous work which suggests these dusty olivines hold a record of the solar nebula magnetic field during the early stages of solar system formation.

\body

## Introduction

The Semarkona meteorite is an LL 3.0 ordinary chondrite, containing some of the most pristine and unequilibrated chondrules. These chondrules contain dusty olivine grains, formed by reduction of olivine ( $(\text{Fe,Mg})_2\text{SiO}_4$ ) in the earliest stages of the solar nebula. These dusty olivines are not thought to have formed by crystallisation within the host chondrule, but represent relict grains of an even earlier time in solar system history, prior to chondrule formation (Leroux et al., 2003). The dusty olivines contain sub-micron sized metallic grains of almost pure Fe kamacite (Uehara and Nakamura, 2006). A recent 3D micromagnetic and tomographic study of the Semarkona meteorite concluded that the majority of stable remanence carriers in dusty olivines were vortex and small MD states (Einsle et al., 2016). Significant research has been undertaken to investigate the credibility of these Fe particles as paleomagnetic carriers of solar nebula magnetic fields (Einsle et al., 2016; Lappe et al., 2011; Shah et al., 2018). The first paleomagnetic measurement of a solar nebula field was captured by a dusty olivine from the Semarkona chondrite, with important implications for the formation of the pre-accretionary disk and the first solid material in the solar system (Fu et al., 2014).

Recent research has also shown that single-vortex (SV) grains can behave like uniaxial single domain (SD) grains, and may in fact be more stable as paleomagnetic recorders (Almeida et al., 2014; Nagy et al., 2017). This is a significant discovery for all fields of paleomagnetic research, since the vast majority of magnetic grains in rocks fall in the vortex to multi-vortex size range from  $\sim 0.1 - 10 \mu\text{m}$  (Roberts et al. 2017). Off-axis electron holography studies have directly imaged vortex behaviour at a range of temperatures and show good agreement with micromagnetic simulations. These results suggest that vortex structures are stable

recorders of both thermoremanent magnetisation, paleodirections and paleointensities (Almeida et al., 2014; Shah et al., 2018).

The aim of this study was to directly image the magnetic response of dusty olivine inclusions under high applied magnetic fields, and thereby assess the validity of micromagnetic simulations that predict high field stability for these particles. Magnetic imaging in high applied fields is extremely challenging using conventional electron-beam techniques (e.g. electron holography) since strong magnetic fields adversely affect the trajectory of electrons through the microscope. For this reason, previous experiments which image vortex states in natural materials have been performed under zero-field conditions (Shah et al., 2018). The soft X-ray transmission microscope at the XM-1 beamline at the Advanced Light Source (Berkeley, California) offers a particularly attractive set up for imaging in applied magnetic fields, since it operates in a photon-in/photon-out regime, therefore magnetic fields may be applied in any orientation without affecting the image. The XM-1 beamline is capable of 15 nm spatial resolution and 70 picosecond temporal resolution (Fischer et al., 2006), allowing the behaviour of the smallest magnetic structures to be imaged.


There have been several successful experiments that utilise X-ray magnetic circular dichroism (XMCD) to image vortex core behaviour with picosecond time resolution (Choe et al., 2004; Guslienko et al., 2006; Raabe et al., 2005). This research focusses on the application of vortex cores as memory devices and uses permalloy thin films with a thickness of ~ 20 nm. These ultra-thin materials provide excellent imaging contrast. Natural samples, on the other hand, are much thicker and more heterogeneous, posing several technical challenges for successful imaging. Here, we show the first results for the response of natural dusty olivines to applied fields of up to ~ 200 mT at room temperature, using soft X-ray transmission microscopy (TXM). Results are presented for five particles from a dusty olivine grain from the Semarkona chondrite. The motion of vortex structures in applied fields is found to be in good agreement with micromagnetic simulations, based on the exact morphology of the particles obtained from electron nanotomography.

A correlative approach is used to interrogate the fundamental properties of nanoscale magnetic particles under strong applied magnetic fields (Figure 1 ). We demonstrate the advantage of combining a variety of experimental techniques to build a comprehensive

dataset for specific particles within a sample. The potential for realistic 3D reconstructions and simulations is also shown, allowing time-consuming experimental procedures to be supplemented by computational results.

## **Methods**

### *Samples*

Iron particles from a dusty olivine grain (sample DOC5 described by Fu et al., 2014), were extracted from a chondrule from the Semarkona LL3.0 ordinary chondrite (Einsle et al., 2016; Fu et al., 2014). Five iron particles formed the focus of the study, the dimensions of which are summarised in Table S1. Three particles were significantly more elongate than the other two, offering the opportunity to investigate the effects of shape anisotropy. The dusty olivine grain was mounted in epoxy on a quartz disc. The disc was subsequently mounted on an SEM stub and carbon coated. The olivine grain needed to be as thin as possible in order to carry out TXM. A focussed ion beam (FIB) lamella was prepared using the FEI Helios Nanolab Dual Beam in the Department of Materials Science and Metallurgy, University of Cambridge. The centre and one edge of the sample were gradually thinned using a stable window configuration (S1). Within the stable window, the sample was gradually thinned into a wedge shape, following the methodology described by (Schaffer et al., 2012). The sample was then mounted on an omniprobe grid with platinum deposition. 

### *Lorentz Microscopy*

Lorentz Microscopy was conducted at the Center for Electron Nanoscopy, Technical University of Denmark. Results were acquired using an FEI Titan 300 keV TEM. Electrons are transmitted through the sample and deflected by its magnetisation. The direction of magnetisation acts to either focus or defocus the electrons, leading to bright or dark spots, respectively.

## *Full-field soft X-ray transmission microscopy*

The samples were measured using full-field soft X-ray transmission microscopy at beamline 6.1.2 (XM-1) at the Advanced Light Source (Lawrence Berkeley National Laboratory, California). This beamline offers a simple set up: X-rays are emitted from a bending magnet source and focussed using two Fresnel zone plates placed at the focal points in front and behind the sample. The sample is mounted on an omniprobe grid, which is taped to the corner of a flat, metal window and then screwed to the sample stage. Samples were imaged in both in-plane (IP) and out-of-plane (OOP) configurations. Magnetic fields were also applied in both orientations. To change from IP to OOP imaging of the sample, the sample was either mounted almost perpendicular ( $\sim 80^\circ$ ) to the direction of transmission (OOP configuration) or on a holder which sits at an angle of  $30^\circ$  to the direction of transmission (Fischer et al., 2001). Magnetic fields are applied using two magnetic pole pieces, which can be mounted to generate a field parallel to the beam (OOP configuration) or perpendicular to the beam (IP configuration). The applied field is generated by applying a current of up to 1 A in either direction across the pole pieces. A 1 A current corresponds to a magnetic field of  $\sim 200$  mT. Magnetic contrast is achieved using X-ray magnetic circular dichroism (XMCD). The bending magnet alters the polarity of the X-rays; by changing the angle of the X-rays to the orbital plane by a few milliradians, 70 % polarisation is achieved. The polarity above the beam centre is the opposite of that below the beam centre, so by selecting different regions of the X-ray beam, opposite polarisations were acquired. Due to inhomogeneity in the beamline, opposite polarisations are not the exact reverse of each other, therefore variation in contrast between opposite polarisations cannot be quantified. Changes in the magnetic signal are also very weak relative to the X-ray absorption of the Fe particles as a whole. In order to generate a visible, quantifiable magnetic contrast, two images acquired in a magnetic field applied in opposite directions (e.g., 10 mT and -10 mT), but with the same polarisation are divided. This gives an intensity of unity anywhere where magnetic contrast has not changed and small variations (mostly  $\pm 5\%$ ) where magnetic structures have shifted (Figure S2). This method therefore produces magnetic contrast generated by the difference in magnetisation between the two applied fields. Forty images were acquired for each applied field direction. Each pair of images is divided and then the average of forty images is taken in order to minimise noise (Figure S3).

### *STEM Nanotomography*

Scanning transmission electron microscope (STEM) tomography was carried out using a FEI Tecnai F20 FEGTEM microscope in the Department of Materials Sciences and Metallurgy, University of Cambridge. High-angle annular dark-field (HAADF) imaging was used, since it almost completely eliminates phase contrast and diffraction effects. This has the advantage of producing an image that is essentially monotonic with thickness and is only sensitive to changes in composition, therefore projection images accurately reflect the genuine particle structure (Midgley and Dunin-Borkowski, 2009; Midgley and Weyland, 2003). Images were acquired every degree between  $\pm 75^\circ$  along a single tilt axis, defined by a protective Pt strip. Images were aligned using FEI's Inspect3D. This experimental set up resulted in a missing wedge of  $30^\circ$ . The Pt strip also partially obscures the two Fe nanoparticles of interest. We reduce reconstruction artefacts due to the missing wedge and the overlapping of the Pt strip at high angles by using a compressive sensing (CS) algorithm developed in the University of Cambridge Electron Microscopy Group (Leary et al., 2013; Saghi et al., 2011).

### *Micromagnetic Simulations*

Micromagnetic simulations were used to investigate the observed **TXM** behaviour of the particles. The shape and size of the particles were accurately reconstructed from the tomography data. The tomographic reconstructions were smoothed using the image processing package ImageJ and converted to a triangular surface mesh. The software package CuBit was then used to convert to a tetrahedral volume mesh. Tetrahedral mesh nodes are distributed at 5 nm intervals throughout the particle. Although this is slightly larger than the exchange length for Fe (3.4 nm), a denser node distribution is too computationally expensive. Nodes at 5 nm intervals provide acceptable resolution for the simple simulations presented here.

Micromagnetic simulations were performed using Micromagnetic Earth Related Rapid Interpreted Language Laboratory (MERRILL) (O Conbhui et al., 2018). A finite-element method and boundary-element method were used to solve for the magnetic scalar potential inside the particle, in order to calculate the demagnetizing energy of the system. The Fe particles were simulated under applied fields in the same orientation as those applied during the **TXM** experiment. Simulations were carried out between -1000 mT and 1000 mT in steps

of 10 mT. At each step, the simulation finds the lowest energy state, taking into account exchange, cubic anisotropy, magnetostatic and demagnetizing energies. Material properties for Fe at 20 °C were assumed: saturation magnetisation,  $M = 1715 \text{ kA m}^{-1}$ ; exchange energy,  $A = 2 \times 10^{-11} \text{ J m}^{-1}$ ; and cubic anisotropy,  $K_1 = 48 \text{ kJ m}^{-3}$  (Muxworthy and Williams, 2015). At the end of each applied field step, magnetic moments within the sample were randomly rotated by up to 30 °; this was used as the starting point for the next applied field step to avoid the simulation terminating in a local energy minimum. These simulations give a 3D representation of the magnetic behaviour of the particle.

In order to directly compare the simulations with the TXM data, representative 2D projections were calculated. Tetrahedral volume meshes were interpolated onto a regularly structured grid of  $100 \times 100 \times 100$  nodes. The magnetic moment at each node in the structured grid is the contribution from all of the surrounding nodes in the tetrahedral volume mesh. The entire stack is then averaged in the z-direction to give a  $100 \times 100$  2D projection of the Fe particle. In the TXM experiments the Fe particles are highly absorbing, with only 20 % of the photons being transmitted. Therefore, a background value is added to the simulated projection to represent this absorption. An image is then generated for qualitative comparison with the TXM data.

## Results

### *Imaging the magnetic structure of nanoscale Fe particles*

Over-focussed (Figure 2a) and under-focussed (Figure 2b) Lorentz images were acquired for two particles. In the over-focussed image, a bright region of contrast runs along the centre of the long-axis of the upper, elongate particle. This particle will herein be referred to as the ‘Kittel particle’ since its domain walls divide the particle into four quadrants forming a Kittel closure structure (Kittel, 1946). The lower, rounded particle has a dark centre and will be referred to as the ‘Vortex particle’ due to its single vortex magnetic structure. The alternate contrast observed in the two particles demonstrates that the magnetisation of each of the particles rotates in opposite senses. The under-focussed image confirms these observations;



the elongate particle has a dark centre, while the particle beneath has a bright centre. The high-resolution contrast sharply defines the interior magnetic structure of these particles.

The same particles that were imaged using Lorentz microscopy were then imaged using TXM (Fig. 5c). Using this method, the lateral shift of the domain wall and/or vortex core in response to the oppositely applied magnetic field is seen as a paired bright/dark feature, as shown schematically in Fig. S2. The particles were imaged under an increasing out-of-plane (OOP) applied magnetic field from 20 to 200 mT (Fig. 6). As the applied field was increased, the observed contrast within the particles increased, corresponding to larger shifts of the interior magnetic structure. The internal structure in the Vortex particle shifts in the opposite direction to the Kittel particle, causing the light and dark contrast to be reversed. This is consistent with results from Lorentz microscopy.

To investigate the response of the internal magnetic structure to the direction of the applied magnetic field, three more particles (Particle 1, Particle 2 and Particle 3) were imaged in one IP and two OOP orientations (Figure 5). The different magnetic response to each applied field direction was observed in the TXM contrast. The IP applied field causes the largest shift of the vortices, since it is applied almost perpendicular to each vortex. For the two OOP applied field directions, the response of the particles depends on their morphology relative to the direction of the small in-plane component of the applied field. A larger shift was observed when the in-plane component of the OOP applied field was perpendicular to the elongate axis of the particles. Particle 2, which has the most equant morphology was the most stable; the single vortex structure only experienced small shifts, even under applied fields of 200 mT.

All of the changes in magnetic structure are confined toward the centre of the particles, most of which exhibit single vortex cores. For all applied field directions and particles, no domain wall annihilation has occurred at 200 mT, suggesting they are still extremely stable under applied fields of this strength.

### *Comparing experimental results with micromagnetic simulations*

In order to compare experimental results with micromagnetic simulations, accurate 3D morphologies of the measured particles were reconstructed using STEM nanotomography (Figure 3). These morphologies were then used with MERRILL to generate 3D micromagnetic simulations of particle behaviour under varying applied magnetic fields. The

3D simulations were then converted to a 2D projection for direct comparison with the TXM experimental data.

Figures 4 and 5 show experimental and simulated TXM images. In all cases the simulations are in good qualitative agreement, although slightly larger shifts are observed for a given applied field strength. Results from micromagnetic simulations can be used to begin to interpret the response of the particles to applied magnetic fields. The hysteresis loops shown in Figure 5 demonstrate how the change in applied field direction and particle morphology influence magnetic behaviour. Domain walls are annihilated at lower applied fields in the IP configuration, or when the in-plane component of the OOP field is aligned along the short axis of elongate particles. Particle 2, which has the most equant morphology, exhibits the most stable behaviour.

Paraview (Ahrens et al., 2005; Ayachit, 2016) was used to visualise how the change in contrast in the processed TXM images corresponds to the actual shift in magnetic structure. Profiles of simulated TXM intensity were taken across the particles (Figure 6). The profiles are asymmetric between the light and dark regions. This implies that the shift in magnetic structure is small, i.e. the change in magnetic structure for positive and negative applied fields overlaps. The magnitude of the TXM signal increases as the particles become more strongly magnetised.

Simulations were run for a larger range of applied field strengths than were investigated experimentally, ranging between  $\pm 1$  T (Figure 5). The applied field strengths for which domain walls are annihilated are shown in Table 1 and are found to exceed 200 mT in all cases.

## **Discussion**

Results show the first direct experimental observations of the magnetic response of vortex states in natural samples to an applied external magnetic field. Fe particles in dusty olivine grains are found to be stable under strong applied fields ( $> 200$  mT). This is in good agreement with recent studies suggesting single-vortex grains may in fact be more stable than SD particles (Nagy et al., 2017). In the following, we discuss the various experimental techniques used to image the magnetic structure of the particles and the merits of combining

multiple techniques with micromagnetic simulations to fully characterize the observed behaviour.

Lorentz microscopy images magnetic contrast within particles using the deflection experienced by electrons as they pass through a region of magnetic induction (Chapman and Scheinfein, 1999). Figure 2 shows the high resolution magnetic structure within the particles. The Lorentz images are much higher resolution than the equivalent TXM images, demonstrating the superiority of the Lorentz method for the direct imaging of the magnetic structure. The magnetic structure of the Kittel particle is revealed in the over-focussed image (Figure 2a), while the magnetic structure of the vortex particle is best seen in the under-focussed image (Figure 2b). This is consistent with the opposite response of each of the particles to an applied magnetic field, shown by the opposite change in contrast in the TXM image (Figure 2c). Although Lorentz microscopy provides better contrast, imaging in the presence of a large magnetic field is experimentally highly challenging.

TXM has an advantage over Lorentz microscopy in allowing direct imaging of the response of magnetic structure to a large applied field. The results presented here demonstrate a proof-of-concept that natural, nanoscale particles can be imaged with a resolution high enough to monitor their response under varying magnetic fields. This technique is already well established for vortex dynamics in permalloys (Kasai et al., 2008). Several experimental challenges were encountered specific to the imaging of natural samples. Because natural samples are thicker and more heterogeneous than idealised permalloys, the magnetic signals from the particles are very small, particularly compared to the high X-ray absorption of the Fe particle as a whole (Figure S2). In order to visualise magnetic structure within the particles, one image must be divided by another in different applied fields. This removes the large absorption step from the Fe particle, which does not change with varying applied field (Figure S3). Magnetic contrast generates a  $< 5\%$  change in intensity, for equal and opposite applied fields up to  $\sim 200$  mT.

In order to compare experimental results to micromagnetic simulations, the exact morphology of the particles must be known. We were able to accurately constrain the morphology of the studied iron particles in the size range  $\sim 200 - 600$  nm using STEM tomography. This allows the influence of a precise morphology on the magnetic response of particles to be simulated under various applied field conditions. Although simple, ellipsoid structures are investigated here, the merits of using this method to investigate the response of more complex

morphologies, which are often encountered in natural samples, e.g. dendrites, are clear (Shaar and Feinberg, 2013).

3D reconstructions highlight the flattened top and bottom of the particles. Particles have to be < 200 nm thick in order to transmit X-rays. This means that the particles studied here, which have a diameter exceeding 200 nm (), cannot be imaged with their natural morphology and must be made planar, hence altering their magnetic behaviour. This is a problem for any experimental technique requiring transmission through extremely thin samples e.g., electron holography (Shah et al., 2018). New imaging methods are currently being developed which use hard X-rays. These higher energy X-rays allow high resolution, temporally-resolved imaging in applied fields for thicker samples with their natural morphology (Falch et al., 2017). There has been one successful study using hard X-rays to image the 3D magnetisation of a synthetic sample (Donnelly et al., 2017). This is extremely promising for future successful imaging of the natural morphology of magnetic carriers.

The micromagnetic simulations are found to be in good agreement with the experimental data. This suggests that the simulations are reliable enough to extend the results to higher applied fields and varying field directions, and could also be used to simulate the natural morphology of particles without the need to plane-off their tops and bottoms. Simulations can also be used to define rock magnetic properties for specific samples. When considering nanoscale inclusions, such as those presented here, experimental methods are extremely challenging, expensive and time consuming. Therefore the ability to enhance experimental data with realistic simulations is important for the success and scope of future nanomagnetic studies.

Another advantage of micromagnetic simulations is the diversity with which the results can be presented. 3D reconstructions of the magnetic behaviour within an individual particle are invaluable for fully interpreting their response (Figure 6c). Experimental images may also be reproduced, such as those acquired during TXM experiments (Figures 4 & 5). Results from electron holography have also been simulated from micromagnetic simulations (Almeida et al., 2014; Conbhuí et al., 2016).

Experimental and simulated TXM results suggest that dusty olivine particles are stable in strong applied fields of at least 200 mT. This applied field is much stronger than any

magnetic field the samples were likely to encounter in the solar system (most planetary-strength magnetic fields are a few tens to hundreds of microtesla). Therefore these results suggest that dusty olivines in the Semarkona meteorite contain extremely stable paleomagnetic recorders, in support of several previous studies (Einsle et al., 2016; Fu et al., 2014; Lappe et al., 2011). We therefore suggest it is likely that Semarkona retains information about the earliest magnetic fields during the solar nebula.

## **Conclusions**

A correlative approach is presented for the direct investigation of nanoscale magnetic properties in dusty olivine particles from the Semarkona meteorite. Lorentz microscopy was used to provide high resolution images of the internal magnetic structure of nanoscale particles. Particles with complex internal structure, such as vortex or Kittel states were then selected for further study. Selected particles were then imaged using TXM to investigate their response under strong applied magnetic fields. STEM nanotomography was subsequently used to create high resolution 3D reconstructions of the particles which were then used to generate realistic micromagnetic simulations which can be directly compared to experimental results. Such realistic simulations minimise the amount of challenging experimental work that must be carried out, since a larger range of experimental conditions can be investigated via simulations. The simulations presented here are in good agreement with the TXM data.

Results of TXM studies and micromagnetic simulations support previous studies which suggest dusty olivines are extremely reliable paleomagnetic recorders. Fe inclusions exhibiting both single vortex and Kittel closure structures are stable in applied fields  $\geq 200$  mT. This is much stronger than any magnetic field naturally generated within the solar system, suggesting it is unlikely dusty olivines have been overprinted by other magnetic fields after acquiring remanence.

This is the first correlative approach resulting in the direct characterisation of the behaviour and internal magnetic structure of nanoparticles in the vortex size range. This is relevant for the majority of paleomagnetic carriers, which exhibit vortex to multi-vortex behaviour. Vortex grains are still poorly understood and essential for furthering the applications of

paleomagnetic study, such as unravelling Earth's earliest paleomagnetic record and interpreting extraterrestrial paleomagnetic signals from meteorites.

### **Acknowledgements**

The research leading to these results has received funding from the European Research Council under the European Union's Seventh Framework Programme (FP/2007-2013) / ERC Grant Agreement No. 320750. We thank Roger Fu and Benjamin Weiss for providing us with samples of the Semarkona chondrite. James Bryson and Ioan Lascu assisted with TXM experiments. Jon Barnard provided advice and assistance for the STEM tomography experiment. Pádraig Ó Conbhuí provided the code to convert 3D micromagnetic simulations to a regular 2D grid.

### **References**

- Ahrens, J., Law, C., Geveci, B., James Ahrens, Charles L. B. Geveci, 2005. Paraview: An end user tool for large data visualization. *Vis. Handb.* 836, 717–731.  
<https://doi.org/10.1016/B978-012387582-2/50038-1>
- Almeida, T.P., Kasama, T., Muxworthy, A.R., Williams, W., Nagy, L., Dunin-Borkowski, R.E., 2014. Observing thermomagnetic stability of nonideal magnetite particles: Good paleomagnetic recorders? *Geophys. Res. Lett.* 41, 7041–7047.  
<https://doi.org/10.1002/2014GL061432>
- Ayachit, U., 2016. *The ParaView Guide*.
- Chapman, J.N., Scheinfein, M.R., 1999. Transmission electron microscopies of magnetic microstructures. *J. Magn. Mater.* 200, 729–740. [https://doi.org/10.1016/S0304-8853\(99\)00317-0](https://doi.org/10.1016/S0304-8853(99)00317-0)
- Choe, S.-B., Acremann, Y., Scholl, A., Bauer, A., Doran, A., Stöhr, J., Padmore, H.A., 2004. Vortex Core - Driven Magnetization Dynamics. *Science* (80-. ). 304, 420–423.
- Conbhuí, P.Ó., Williams, W., Nagy, L., 2016. Simulated electron holography of PSD particles. *EGU Gen. Assem.* 18.
- Donnelly, C., Guizar-Sicairos, M., Scagnoli, V., Gliga, S., Holler, M., Raabe, J., Heyderman, L.J., 2017. Three-dimensional magnetization structures revealed with X-ray vector nanotomography. *Nature* 547, 328–331. <https://doi.org/10.1038/nature23006>
- Einsle, J.F., Harrison, R.J., Kasama, T., O Conbhui, P., Fabian, K., Williams, W., Woodland, L., Fu, R.R., Weiss, B.P., Midgley, P.A., 2016. Multi-scale three-dimensional

- characterization of iron particles in dusty olivine: Implications for paleomagnetism of chondritic meteorites. *Am. Mineral.* 101, 2070–2084.  
<https://doi.org/10.2138/am.2010.3521>
- Falch, K.V., Casari, D., Di Michiel, M., Detlefs, C., Snigireva, A., Snigireva, I., Honkimäki, V., Mathiesen, R.H., 2017. In situ hard X-ray transmission microscopy for material science. *J. Mater. Sci.* 52, 3497–3507. <https://doi.org/10.1007/s10853-016-0643-8>
- Fischer, P., Eimuller T., Schutz, G., Kohler, M., Bayreuther, G., Denbeaux, G., Attwood, D., 2001. Study of in-plane magnetic domains with magnetic transmission x-ray microscopy. *J. Appl. Phys.* 89, 7159–7161. <https://doi.org/10.1063/1.1355333>
- Fischer, P., Kim, D.-H., Chao, W., Liddle, J.A., Anderson, E.H., Attwood, D.T., 2006. Soft X-ray microscopy of nanomagnetism. *Mater. Today* 9, 26–33.  
[https://doi.org/10.1016/S1369-7021\(05\)71335-3](https://doi.org/10.1016/S1369-7021(05)71335-3)
- Fu, R.R., Weiss, B.P., Lima, E.A., Richard, J., Bai, X.-N., Desch, S.J., Ebel, D.S., Suavet, C., Wang, H., Glenn, D., Sage, D. Le, Kasama, T., Walsworth, R.L., Kuan, A.T., 2014. Solar nebula magnetic fields recorded in the Semarkona meteorite. *Science* (80-. ). 346, 1–9.
- Gusliencko, K.Y., Han, X.F., Keavney, D.J., Divan, R., Bader, S.D., 2006. Magnetic vortex core dynamics in cylindrical ferromagnetic dots. *Phys. Rev. Lett.* 96, 1–4.  
<https://doi.org/10.1103/PhysRevLett.96.067205>
- Kasai, S., Fischer, P., Im, M.Y., Yamada, K., Nakatani, Y., Kobayashi, K., Kohno, H., Ono, T., 2008. Probing the Spin polarization of current by soft X-ray imaging of current-induced magnetic vortex dynamics. *Phys. Rev. Lett.* 101, 1–4.  
<https://doi.org/10.1103/PhysRevLett.101.237203>
- Kittel, C., 1946. Theory of the structure of ferromagnetic domains in films and small particles. *Phys. Rev.* 70, 965–971. <https://doi.org/10.1103/PhysRev.70.965>
- Lappe, S.C.L.L., Church, N.S., Kasama, T., Da Silva Fanta, A.B., Bromiley, G., Dunin-Borkowski, R.E., Feinberg, J.M., Russell, S., Harrison, R.J., 2011. Mineral magnetism of dusty olivine: A credible recorder of pre-accretionary remanence. *Geochemistry, Geophys. Geosystems* 12, 1–20. <https://doi.org/10.1029/2011GC003811>
- Leary, R., Saghi, Z., Midgley, P.A., Holland, D.J., 2013. Compressed sensing electron tomography. *Ultramicroscopy* 131, 70–91.  
<https://doi.org/10.1016/j.ultramic.2013.03.019>
- Leroux, H., Libourel, G., Lemelle, L., Guyot, F., 2003. Experimental study and TEM characterization of dusty olivines in chondrites: Evidence for formation by in situ

- reduction. *Meteorit. Planet. Sci.* 38, 81–94. <https://doi.org/10.1111/j.1945-5100.2003.tb01047.x>
- Midgley, P.A., Dunin-Borkowski, R.E., 2009. Electron tomography and holography in materials science. *Nat. Mater.* 8, 271–280. <https://doi.org/10.1038/nmat2406>
- Midgley, P.A., Weyland, M., 2003. 3D electron microscopy in the physical sciences: The development of Z-contrast and EFTEM tomography. *Ultramicroscopy* 96, 413–431. [https://doi.org/10.1016/S0304-3991\(03\)00105-0](https://doi.org/10.1016/S0304-3991(03)00105-0)
- Muxworthy, A.R., Williams, W., 2015. Critical single-domain grain sizes in elongated iron particles: implications for meteoritic and lunar magnetism. *Geophys. J. Int.* 202, 578–583. <https://doi.org/10.1093/gji/ggv180>
- Nagy, L., Williams, W., Muxworthy, A.R., Fabian, K., Almeida, T.P., Conbhuí, O., Shcherbakov, V.P., 2017. Stability of equidimensional pseudo-single-domain magnetite over billion-year timescales. <https://doi.org/10.1073/pnas.1708344114>
- O Conbhui, P., Williams, W., Fabian, K., Ridley, P., Muxworthy, A.R., 2018. MERRILL : Micromagnetic Earth Related Robust Interpreted Language Laboratory. *Geochem. Geophys. Geosyst.*
- Raabe, J., Quitmann, C., Back, C.H., Nolting, F., Johnson, S., Buehler, C., 2005. Quantitative analysis of magnetic excitations in landau flux-closure structures using synchrotron-radiation microscopy. *Phys. Rev. Lett.* 94, 1–4. <https://doi.org/10.1103/PhysRevLett.94.217204>
- Saghi, Z., Holland, D.J., Leary, R., Falqui, A., Bertoni, G., Sederman, A.J., Gladden, L.F., Midgley, P.A., 2011. Three-dimensional morphology of iron oxide nanoparticles with reactive concave surfaces. A compressed sensing-electron tomography (CS-ET) approach. *Nano Lett.* 11, 4666–4673. <https://doi.org/10.1021/nl202253a>
- Schaffer, M., Schaffer, B., Ramasse, Q., 2012. Sample preparation for atomic-resolution STEM at low voltages by FIB. *Ultramicroscopy* 114, 62–71. <https://doi.org/10.1016/j.ultramic.2012.01.005>
- Shaar, R., Feinberg, J.M., 2013. Rock magnetic properties of dendrites: Insights from MFM imaging and implications for paleomagnetic studies. *Geochemistry, Geophys. Geosystems* 14, 407–421. <https://doi.org/10.1002/ggge.20053>
- Shah, J., Williams, W., Almeida, T.P., Nagy, L., Muxworthy, A.R., Kovács, A., Valdez-Grijalva, M.A., Fabian, K., Russell, S.S., Genge, M.J., Dunin-Borkowski, R.E., 2018. The oldest magnetic record in our solar system identified using nanometric imaging and numerical modeling. *Nat. Commun.* 9, 9–14. <https://doi.org/10.1038/s41467-018-03613->



Uehara, M., Nakamura, N., 2006. Experimental constraints on magnetic stability of chondrules and the paleomagnetic significance of dusty olivines. *Earth Planet. Sci. Lett.* 250, 292–305. <https://doi.org/10.1016/j.epsl.2006.07.042>

## Figures and Tables

Particle	Applied Field (mT)			
	OOP	IP	OOP1	OOP2
<b>Vortex</b>	> 1000	-	-	-
<b>Kittel</b>	780	-	-	-
<b>Particle1</b>	-	370	370	510
<b>Particle2</b>	-	550	490	480
<b>Particle3</b>	-	330	330	490

**Table 1** Applied field strengths leading to annihilation of domain walls from micromagnetic simulations

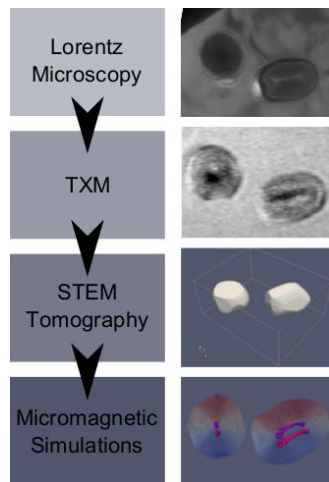


**Figure 1** A correlative approach is demonstrated in order to investigate the fundamental properties of nanoscale magnetic particles. Results of Lorentz microscopy (Fu et al., 2014) are combined with results on the same particles using transmission X-ray microscopy (TXM). A 3D reconstruction of the imaged particles is then generated using STEM tomography. These 3D reconstructions are used to carry out realistic micromagnetic simulations using MERRILL.

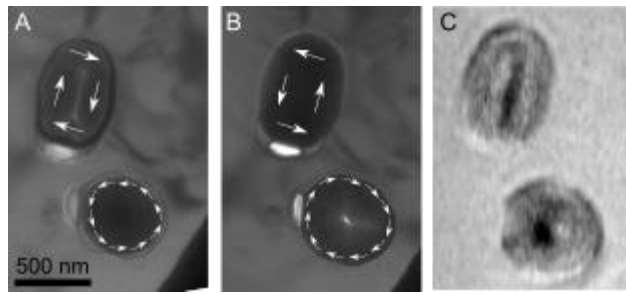


**Figure 2** (a) An over-focussed Lorentz image (b) An under-focussed Lorentz image (c) A TXM image. Similar contrast is observed in particles A and B.

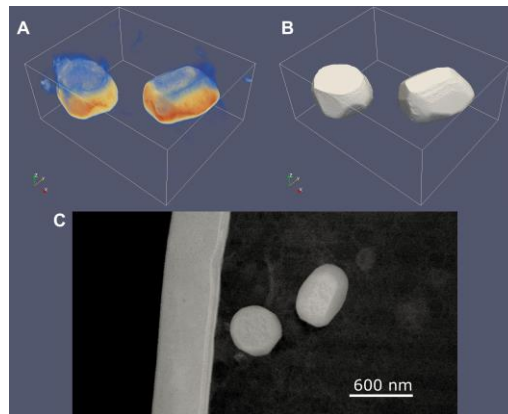


**Figure 3** Tomographic reconstruction of the Kittel and Vortex particles. (a) Elongate artefacts (shown in blue) can be observed in the direction of the missing wedge. (b) Shows the resulting 3D reconstruction. (c) Shows the protective platinum strip, aligned approximately along the tilt axis.

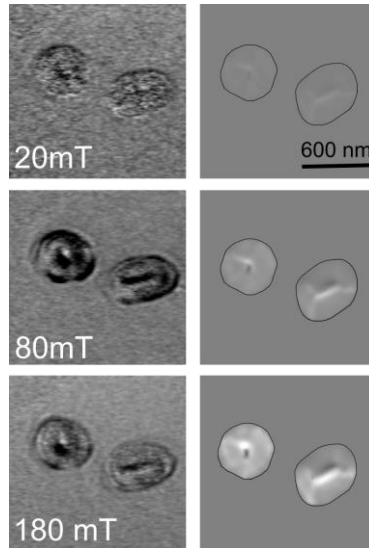


**Figure 4** The TXM images are in good agreement with simulations for the same projection. The grey background has a uniform value of 1, i.e., there is no difference between the divided images in these regions. Background noise has been removed.

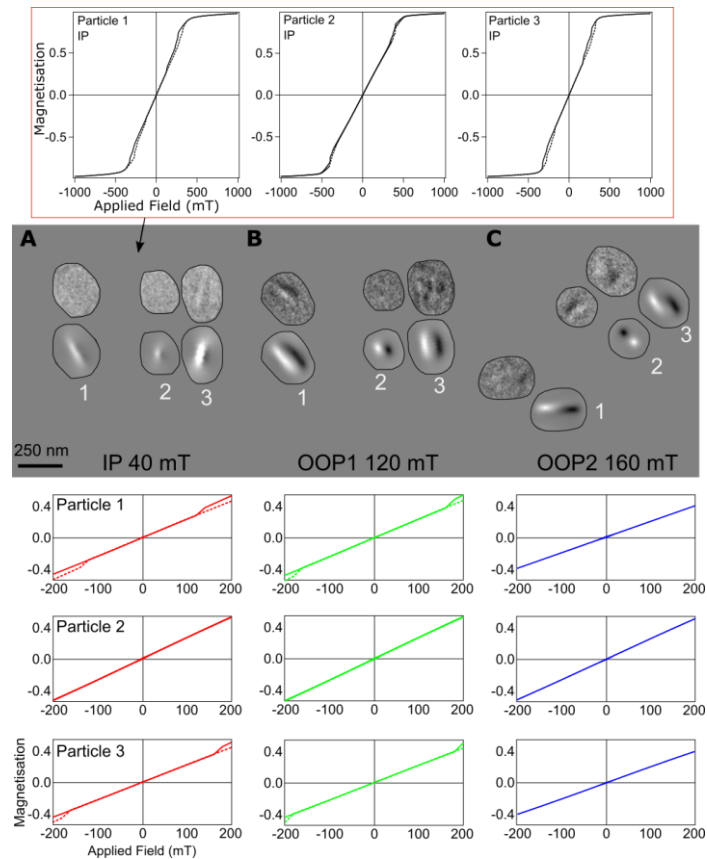


**Figure 5** Examples of TXM images and corresponding simulations are shown for three more particles in a dusty olivine from the Semarkona chondrite. (a) An in-plane applied field, with full hysteresis loops ( $\pm 1$  T) shown above. (b) An out-of-plane applied field (orientation 1). (c) The second orientation for an out-of-plane applied field. Below each image are the sub-hysteresis loops ( $\pm 200$  mT) calculated from micromagnetic simulations for each particle.

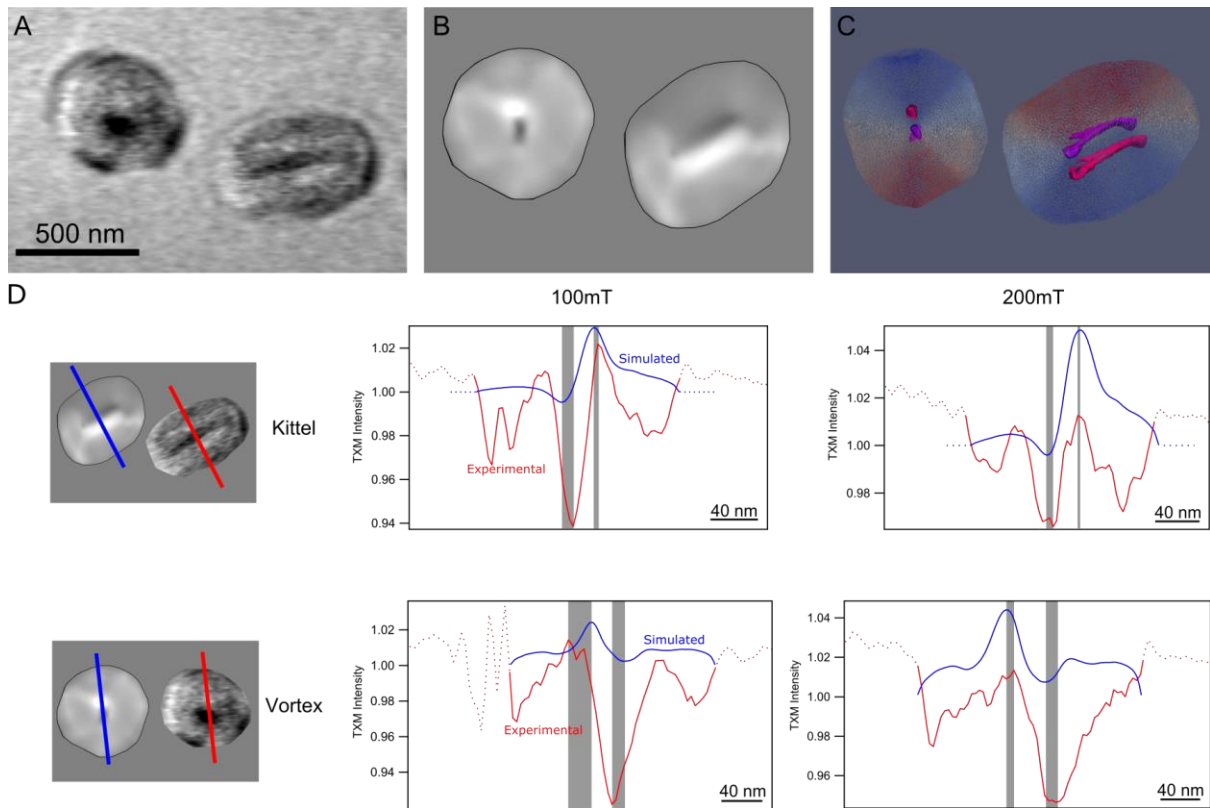


**Figure 6** (a) A TXM image for a 200 mT OOP applied field. (b) The corresponding simulated TXM image, from the micromagnetic simulations. (c) A 3D visualisation in Paraview of the actual change in magnetic structure in response to an applied field. The purple and pink regions are selected as lines of constant moment and correspond to an applied field of -200 mT and 200 mT respectively. (d) Red lines represent profiles across TXM images and blue lines represent profiles across simulated images. Grey bars show the misfit between simulated and experimental peaks and troughs, which represent the offset in magnetic structure for a given applied field.